Received: 14 June 2023 | Revised: 19 July 2023 | Accepted: 20 July 2023

DOI: 10.1002/pro.4734

RESEARCH ARTICLE

THE PROTEIN SOCIETY WILEY

Role and structure of the small subunit forming heterodimers with laccase-like enzymes

Pablo Aza[1] | **Dolores Linde**[1] | **Gonzalo Molpeceres**[1] | **Jesper Vind**[2] | **F. Javier Medrano**[1] | **Susana Camarero**[1]

[1]Centro de Investigaciones Biológicas Margarita Salas, CSIC, Madrid, Spain

[2]Novozymes A/S, Kongens Lyngby, Denmark

Correspondence
F. Javier Medrano and Susana Camarero, Centro de Investigaciones Biológicas Margarita Salas, CSIC, Ramiro de Maeztu 9, 28040 Madrid, Spain.
Email: fjmedrano@cib.csic.es and susanacam@cib.csic.es

Funding information
Bio-Based Industries Joint Undertaking, Grant/Award Number: GA 792070; Fundación Tatiana Pérez de Guzmán el Bueno; Ministerio de Ciencia e Innovación, Grant/Award Number: PID2021-126384OB-I00; Ministerio de Economía y Competitividad, Grant/Award Number: BIO2017-86559-R; Ministerio de Universidades; CSIC Interdisciplinary Platform for Sustainable Plastics toward a Circular Economy (PTI-SusPlast+)

Review Editor: Jeanine Amacher

Abstract

Unlike laccases sensu stricto, which are usually monomeric enzymes, laccase-like enzymes recently re-classified as Novel Laccases (NLACs) are characterized by the formation of heterodimers with small proteins (subunits) of unknown function. Here the NLAC from *Pleurotus eryngii* (PeNL) and a small protein selected from the fungal genome, that is homologous to reported POXA3 from *Pleurotus ostreatus,* were produced in *Aspergillus oryzae* separately or together. The two proteins interacted regardless of whether the small subunit was co-expressed or exogenously added to the enzyme. The stability and catalytic activity of PeNL was significantly enhanced in the presence of the small subunit. Size exclusion chromatography-multi angle light scattering (SEC-MALS) analysis confirmed that the complex PeNL-ss is a heterodimer of 77.4 kDa. The crystallographic structure of the small protein expressed in *Escherichia coli* was solved at 1.6 Å resolution. This is the first structure elucidated of a small subunit of a NLAC. The helix bundle structure of the small subunit accommodates well with the enzyme model structure, including interactions with specific regions of NLACs and some amino acid residues of the substrate-binding loops.

KEYWORDS
crystal structure, heterodimer, novel laccase, *Pleurotus eryngii*, small subunit

1 | INTRODUCTION

Laccases are Multicopper Oxidases (MCOs) distributed in bacteria, plants and fungi, where they participate in diverse biological functions (Janusz et al., 2020). In fungi, they are typically monomeric enzymes formed by three cupredoxin-type domains (Hakulinen & Rouvinen, 2015; Zhukova et al., 2010). Fungal laccases oxidize a wide range of organic substrates such as substituted phenols and aryl amines, benzenethiols, aromatic N-heterocycles, and so forth (Baldrian, 2006; Hakulinen & Rouvinen, 2015; Xu, 1996). In particular, certain laccases secreted by basidiomicete fungi such as PM1 (De Salas et al., 2019) show superior oxidation capabilities on a wider range of recalcitrant compounds and lignin, making them particularly relevant in biotechnology, with applications in pulp & paper, food and textile industries, bioremediation, and organic chemistry, including drug synthesis (Riva, 2006; De Salas & Camarero, 2021).

Laccase activity lies on four catalytic copper ions coordinated by 10 conserved histidine and one cysteine

residues. The coppers are classified as one T1 copper placed near the substrate binding pocket, and the trinuclear cluster (TNC) formed by one T2 copper and the binuclear T3 centre. The T1 copper accepts four electrons from the substrate, which are rapidly transferred through the copper ligands to the TNC for the reduction of O_2 to H_2O (Baldrian, 2006; Hakulinen & Rouvinen, 2015; Xu, 1996). Conserved acidic residues also play a crucial role in the catalysis: (i) an aspartic acid (D205 numbering according to PM1 laccase-PM1L-, Pardo et al., 2016) assists the proton subtraction during one-electron oxidation of phenols at the T1 site (with an histidine mediating the electron transfer to T1 copper (Galli et al., 2013); and (ii) D77 and D453 (PM1L numbering) aid in the proton transfer during oxygen reduction at the TNC (Jones & Solomon, 2015).

To some extent, the efficiency in laccase oxidation is driven by the redox potential of T1 copper. Fungal laccases, particularly those secreted by white-rot basidiomycete fungi, show the highest redox potentials reported so-far (Cambria et al., 2012; Shleev et al., 2004; Xu et al., 1998). Although laccases share a similar oxidation mechanism and conserved copper binding motifs (Giardina et al., 2010; Sekretaryova et al., 2019), their low sequence similarity and broad oxidative spectrum (with overlapping activities with other MCOs) hinder their proper classification. In the last years, the steady growth of computational tools and access to microbial genomes have help to explore the complexity of the MCO superfamily, helping to confine the term "laccases" to a more accurate set of sequences (Kumar et al., 2003). A recent comparative analysis of 52 basidiomycete genomes addressed MCOs classification from a phylogenetic perspective, so that new clusters of laccase-like enzymes, separated from laccases sensu stricto, were identified (Ruiz-Dueñas et al., 2021). One of them is the Novel Laccases (NLACs) cluster which are not found in the order Polyporales, but are distributed among Agaricales and Russulales (Ruiz-Dueñas et al., 2021). NLACs have structural determinants that distinguish them from other laccase-like families. For instance, the aforementioned D205 residue conserved in laccases sensu stricto is substituted by an arginine in NLACs (Galli et al., 2013).

The most extensively studied NLAC member is the so-called POXA3 laccase from *Pleurotus ostreatus*. It was first described as an atypical laccase (Palmieri et al., 2003), and later characterized once produced in *Kluyveromyces lactis* (Faraco et al., 2008). POXA3 forms a heterodimer consisting of a large subunit (the enzyme) and a small subunit with unknown activity (Giardina et al., 2007). The small protein was reported to favorably contribute to the thermostability of the heterodimer (Faraco et al., 2008). A recent study of an enzyme and a small subunit from *Pleurotus eryngii var. ferulae*, homologous to POXA3, showed higher enzyme stability and better activity in the presence of the small subunit. The overexpression of the latter resulted in conformational changes at the mycelial wall level, that seemed to facilitate laccase secretion (Zhang et al., 2021). However, the function of these small proteins remains unknown. Attempts to solve their structure also resulted unsuccessful because their sequences do not show significant homology to any other protein or domain described so far (Ferraroni et al., 2014).

Another member of the NLAC family, initially isolated from the liquid extracts of *Pleurotus eryngii* cultures and described as a laccase (Muñoz et al., 1997a,b), was later identified in the fungal genome (Joint Genome Institute, JGI, ID 1521536) and re-classified as a NLAC according to its phylogenetic origin and sequence/structure features (Ruiz-Dueñas et al., 2021). The enzyme was among the most abundant proteins of the secretome of the fungus grown on a lignocellulosic substrate (Peña et al., 2021), and it was later engineered to enhance its recombinant expression in *Saccharomyces cerevisiae* (Aza, De Salas, et al., 2021a).

In this work, we study the complex formed by this NLAC from *P. eryngii*, PeNL, with a small protein identified in the genome of the fungus. The effect of the small subunit on the stability and activity of PeNL was assayed by co-transformation of both proteins in *Aspergillus oryzae* or by exogenous addition of the small subunit to the NLAC. Finally, the crystal structure of the small subunit (expressed in *E. coli*) and the heterodimeric complex formed by PeNL and the small subunit are described.

2 | RESULTS

2.1 | Expression in *A. oryzae* of the NLAC and small protein of *P. eryngii*

The CDS of PeNL was obtained in a previous work (Aza, De Salas, et al., 2021a). Of the two entries of putative small proteins found in *P. eryngii* genome (JGI ID: 1505570 and 1468497) homologous to the two small subunits of *P. ostreatus*, we selected the one (JGI ID 1468497) with highest sequence identity with the POXA3 subunit with GenBank ID: CAL64898.

The enzyme PeNL and the small subunit were expressed in *A. oryzae*, given the potential of this fungus to over-express eukaryotic proteins (Piscitelli et al., 2010), including basidiomycete MCOs (Aza et al., 2023; De Salas et al., 2016, 2019). To evaluate the effect of the small subunit and the formation of the complex with PeNL, we obtained three types of clones that were cultured in

flasks: (i) *A. oryzae* expressing the NLAC alone (PeNL); (ii) *A. oryzae* transformed with the small subunit alone (small); and (iii) *A. oryzae* co-transformed with PeNL and the small subunit through homologous integrative recombination to induce the formation of the complex (PeNL-ss).

Those clones producing the NLAC (PeNL and PeNL-ss) were cultured in flask separately. In addition, to provide extra amount of the small protein they were co-cultured with the *A. oryzae* clone producing the small subunit alone (small) (Figure 1a). All cultures showed secreted laccase activity after 72 h. However, the enzyme expressed alone did not show activity after incubation at 50°C for 10 min, whereas in the presence of the small subunit, residual activities from 54% to 85% were found (Figure 1b). The highest activity after heat treatment was observed when *A. oryzae* expressing the PeNL-ss complex was co-cultured with the clone producing the small protein (PeNL-ss + Small, Figure 1).

2.2 | Stability of PeNL and PeNL-ss

The enzyme was produced alone (PeNL) or together with the small subunit (PeNL-ss), purified and characterized. PeNL-ss was obtained from the co-culture of *A. oryzae* expressing the complex with the clone expressing the small protein alone (PeNL-ss + Small). The two bands observed in the SDS-PAGE of the purified PeNL-ss corresponded respectively to the molecular weights of the mature PeNL (55 kDa) and the small subunit (17 kDa) (Figure S1). The tolerance to temperature of the enzyme alone (PeNL) or complexed (PeNL-ss) was evaluated in a T50 (10 min) assay. PeNL exhibited a T50 of 43.3°C that was increased to 59.5°C in PeNL-ss (Figure 2).

Then, thermal stability of purified PeNL and PeNL-ss at longer times (0–24 h) of incubation at 30, 40, and 50°C

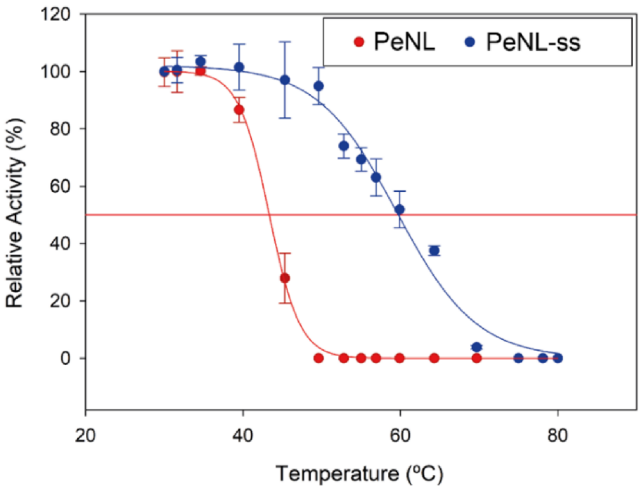

FIGURE 2 T50 (10 min) curves for the monomeric enzyme (PeNL) or complexed with the small subunit (PeNL-ss). Error bars indicate standard deviation for triplicates.

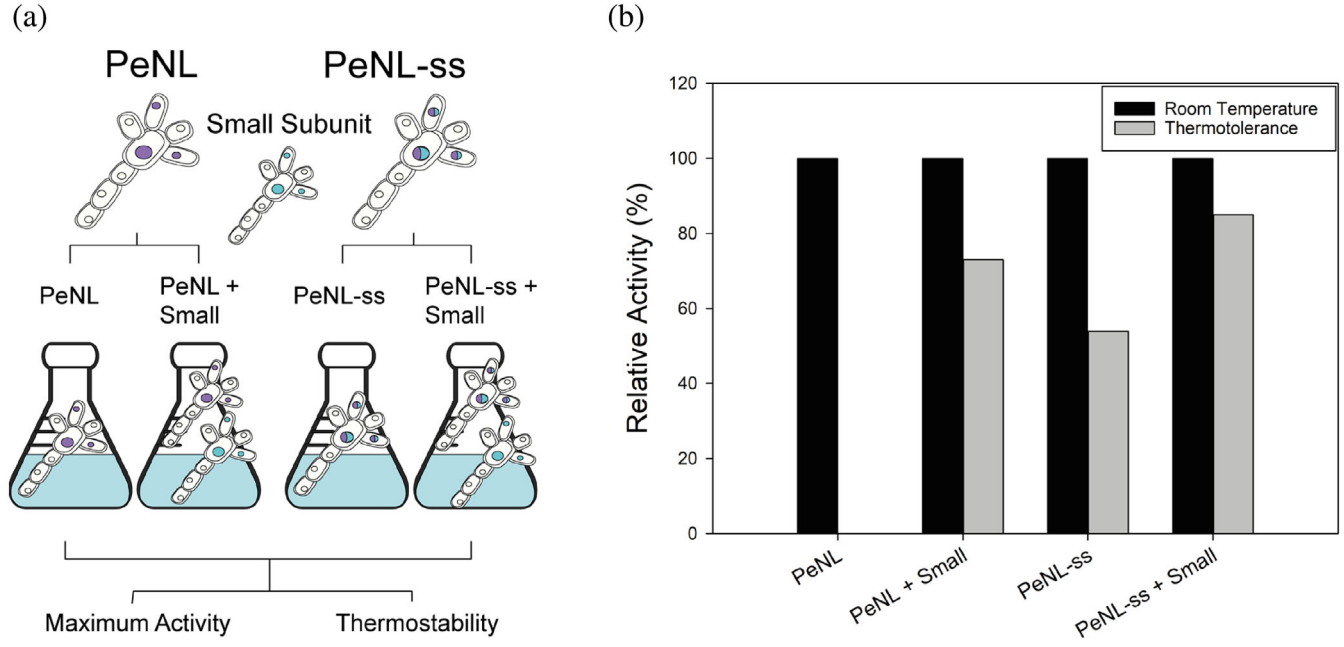

FIGURE 1 (a) Scheme of the experimental design followed to assess the effect of the small subunit in PeNL. *Aspergillus oryzae* transformed with PeNL and/or the small protein were cultured in flasks as follows (from left to right): clone expressing PeNL, co-culture of clones producing PeNL and the small subunit separately (PeNL+ Small), clone expressing the complex PeNL-ss, and co-culture of the latter with that expressing the small protein (PeNL-ss + Small). (b) Laccase activities after incubation at 50°C for 10 min (gray bars) were defined as a percentage of the initial activity (black bars). The values were obtained from duplicate cultures.

was determined (Figure 3). The thermostability of the complex was markedly superior to that of the monomeric enzyme. PeNL barely retained 5% activity after 5 h at 30°C, and no activity was detected after 1 h at temperature ≥40°C (Figure 3a). In contrast, PeNL-ss retained 70% activity after 24 h at 30°C, around 10%–20% after 5 h at 50°C or 24 h at 40°C (Figure 3b).

PeNL showed good tolerance to neutral and alkaline pH but was unstable at acidic pH. PeNL-ss showed same high stability at pH 7 and 9, and notably improved stability at pH 5 (Figure 4).

Finally, we observed important differences in the tolerance of PeNL and PeNL-ss to the presence of ethanol, DMSO and SDS (Figure 5). The enzyme alone was completely inactivated at time zero in 40% ethanol or 0.1% SDS, whereas it retains almost 100% activity after 24 h in 40% DMSO, and around 20% activity after 3 h in 60% DMSO. By contrast, the complex showed 25% of

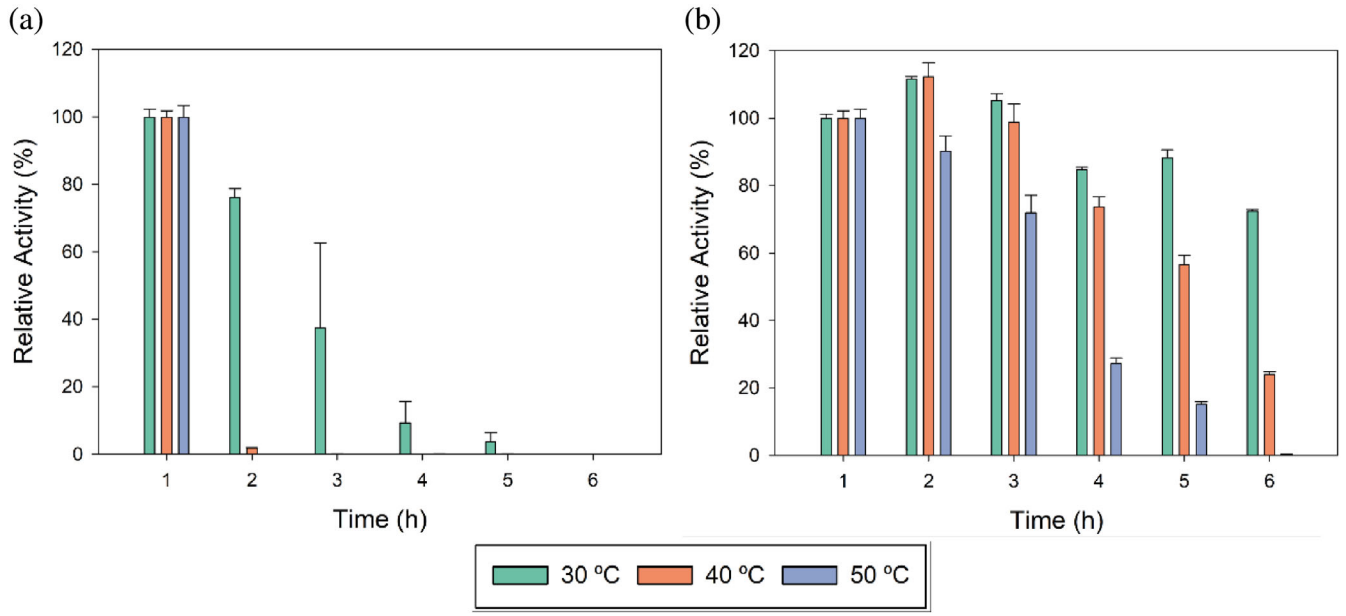

FIGURE 3 Long-term thermal stability of PeNL (a) and PeNL-ss (b). Activities after incubation at 30, 40, and 50°C are indicated as a percentage of the initial activity. Error bars indicate standard deviation for triplicates.

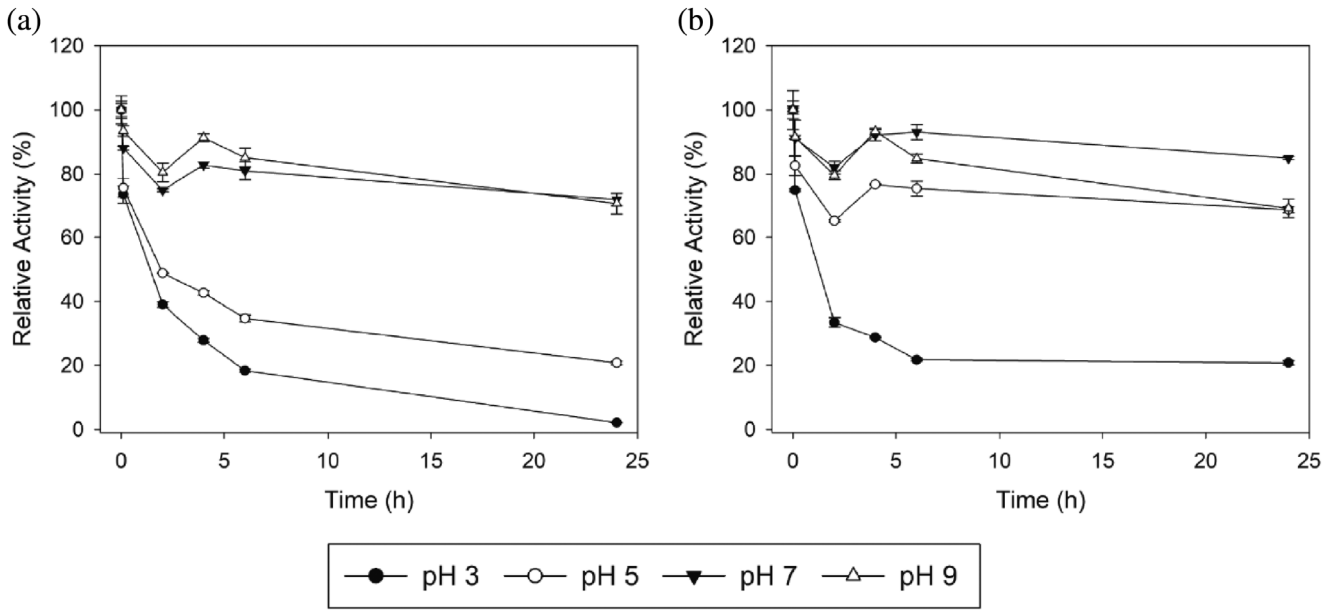

FIGURE 4 Long-term pH stability of PeNL (a) and PeNL-ss (b). Activities after incubation at pH 3, 5, 7, and 9 at 20°C are indicated as a percentage of the initial activity. Error bars indicate standard deviation for triplicates.

activity after 6 h in 40% ethanol and 100% in 0.1% SDS after 24 h.

2.3 | Optimum pH and catalytic properties of PeNL and PeNL-ss

The activity as a function of pH was similar for the monomeric or heteromeric enzyme (Figure S2). In both cases, a sharp peak of activity was found at pH 4 with ABTS.

As for the catalytic constants with typical laccase substrates, PeNL and PeNL-ss showed good affinity for ABTS; the k_{cat} for ABTS of PeNL-ss was significantly higher (Table 1). The enzyme alone barely oxidized DMP, with very poor affinity for this substrate and very low k_{cat}, whereas the k_{cat} of PeNL-ss with DMP was eight times higher. Finally, PeNL was unable to oxidize DMPD, and even though we detected some activity with the complex PeNL-ss, the high variance of the replicates impeded to obtain reproducible catalytic constants.

In an attempt to assess the influence of R211 (equivalent to D205 in PM1L) on phenol oxidation, we obtained the PeNL $_{R211D}$ variant, which showed four-times higher oxidation activity with DMP than PeNL, confirming the involvement of this residue in the oxidation of phenolic substrates (Figure S3).

Due to the lack of sufficient amount of PeNL and PeNL-ss complex from *A. oryzae* we were not able to crystallize them. Alternatively, we successfully produced the small subunit in soluble form in *E. coli*, and purified it using an His-Tag for structural studies. To test whether the recombinant small subunit produced in the bacterium was properly folded and functional, it was purified and incubated with the PeNL produced in *A. oryzae* for 10 min at 60°C. The higher activity of PeNL in the presence of the small subunit proved the functionality of the recombinant small subunit produced in *E. coli* and the in vitro formation of the complex with the enzyme produced in *A. oryzae* (Figure S4).

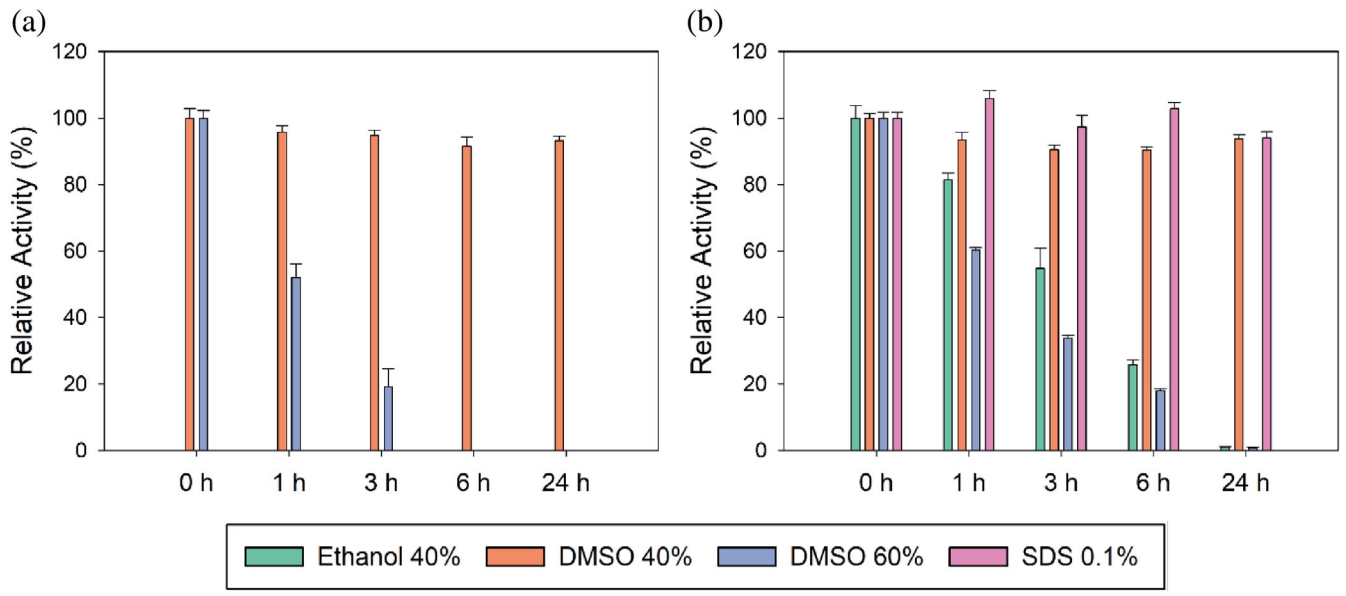

FIGURE 5 Long-term stability of PeNL (a) and PeNL-ss (b) in organic solvents. Activities after enzyme incubation in 40% or 60% ethanol, 60% DMSO or 0.1% SDS are indicated as a percentage of the initial activity. Error bars indicate standard deviation for triplicates.

TABLE 1 Catalytic constants for the oxidation of ABTS and DMP by the enzyme alone (PeNL) or complexed with the small protein (PeNL-ss).

	PeNL			PeNL-ss		
	K_M (mM)	k_{cat} (s^{-1})	k_{cat}/K_M (s^{-1} mM^{-1})	K_M (mM)	k_{cat} (s^{-1})	k_{cat}/K_M (s^{-1} mM^{-1})
ABTS	0.052 ± 0.003	51 ± 1	980 ± 1	0.071 ± 0.005	184 ± 5	2591 ± 5
DMP	4.10 ± 0.54	1.65 ± 0.07	0.40 ± 0.54	8.8 ± 0.5	14.0 ± 0.3	1.60 ± 0.64

2.4 | Structure of the small subunit of *P. eryngii*

The small subunit was successfully crystallized, and its structure determined (PDB ID 8PAQ), at 1.6 Å resolution, with the assistance of Alphafold2 model. The monomer is a helix bundle made up by four helices and three short helices interacting with helices α-3 and α-4 (Figure 6a). The electrostatic surface of the monomer is shown in Figure 6b. The surface of the side made up by α-1 and α-3 (left, oriented as the left figure of panel A) has the bottom two thirds with a hydrophobic character, while the upper third has a relative negative charge (Figure 6b, left). When rotated 130 degrees (Figure 6b, right), we can observe that the surface of helices α-1, α-2 and α-3 has a relative negative charge on the bottom half, while the upper half has relative negative (red), positive (blue), and hydrophobic (white) patches.

The asymmetric unit of the crystal is composed by two monomers that interact through the surface made up by helices α-1 and α-3 forming an X shape, leaving the two ends of the monomers free (Figure S5A). The residues involved in this interaction are mostly of marked hydrophobic character (Figure S5B,C). The analysis of the interaction surface analyzed by the program PISA (https://www.ebi.ac.uk/pdbe/pisa/) (Krissinel & Henrick, 2007) indicates a possible dimeric quaternary structure with total buried area of 1320 Å^2 with a total surface area for the complex of 13,660 Å^2. The solvent free energy change is −14 kcal/mol.

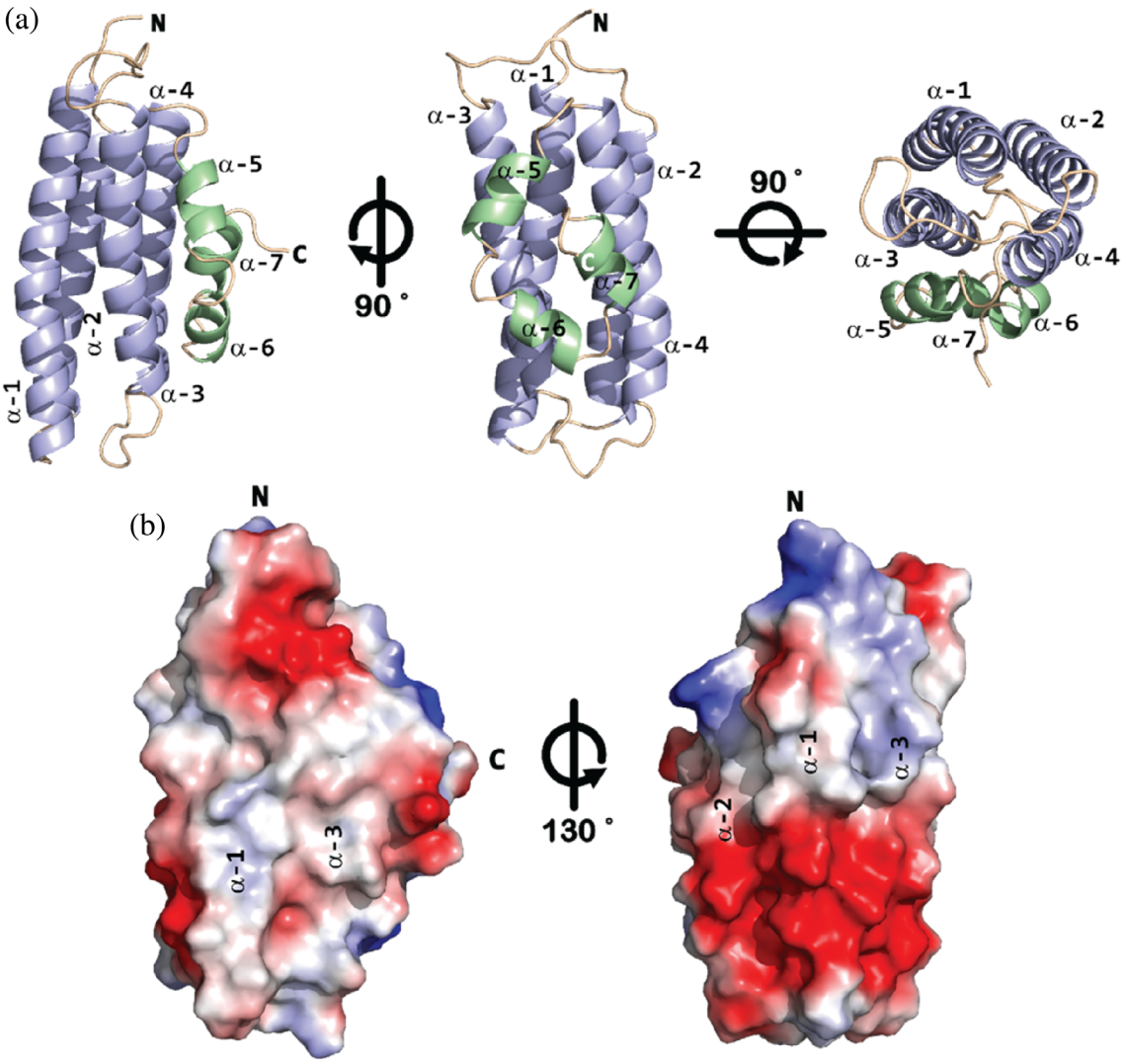

FIGURE 6 Structure of the small subunit of PeNL. (a) Cartoon representation. The protein is made up by a four-helix bundle (light blue) and three short helices (pale green) located at the surface of helices α-3 and α-4. (b) Electrostatic surface. The two orientations show that the surface made up by α-1 and α-3 (left figure, oriented as the left figure of panel (a) has the bottom two thirds with a hydrophobic character (white), while the up third has a relative negative charge (red). The orientation on the right figure of panel (b) shows that the bottom half has a relative negative charge, while the upper half does not present any specific charge.

2.5 | Oligomerization state studies of PeNL and small protein

In order to obtain more information about the arrangement of the small and the catalytic subunits and its quaternary structure, we carried out a prediction of the structure of both subunits using AlphaFold2 (Jumper et al., 2021; Varadi et al., 2022). The predicted structure was a heterodimer with a very favorable interaction surface (Figure 7a). This model of the heterodimer presents a high degree of confidence for most of both proteins (Figure S6). PeNL has two loops showing a lower degree of confidence (higher than 50), while the model of the small subunit presents two loops with a low degree of confidence (lower than 50). This indicates that the models are good. The large (catalytic) subunit embraces the small subunit with some elements of its structure surrounding the small subunit (Figure 7b). The interaction surface of PeNL is concave and accommodates nicely the small subunit (Figure 7c). The small subunit interacts with PeNL all along the structure, including a hydrophobic region and other interactions such as a specific interaction between the negatively charged region of the small subunit with a positively charged region of the large subunit (Figure 7c, circles).

There is a clear discrepancy between the predicted PeNL-ss heterodimer and the crystallographic homodimeric structure of the small subunit. According to the prediction, the small subunit cannot be a dimer in solution. The interaction surface between the monomers in the crystal structure is the same interaction surface of the heterodimer. In order to solve this discrepancy, we carried out Size exclusion chromatography-multi angle light scattering (SEC-MALS) experiments to determine the states of the PeNL-ss complex and of the small subunit in solution. The elution profiles suggested the presence of only one species for each sample (Figure S7). The calculated molecular masses were 77,390 ± 2322 Da for the

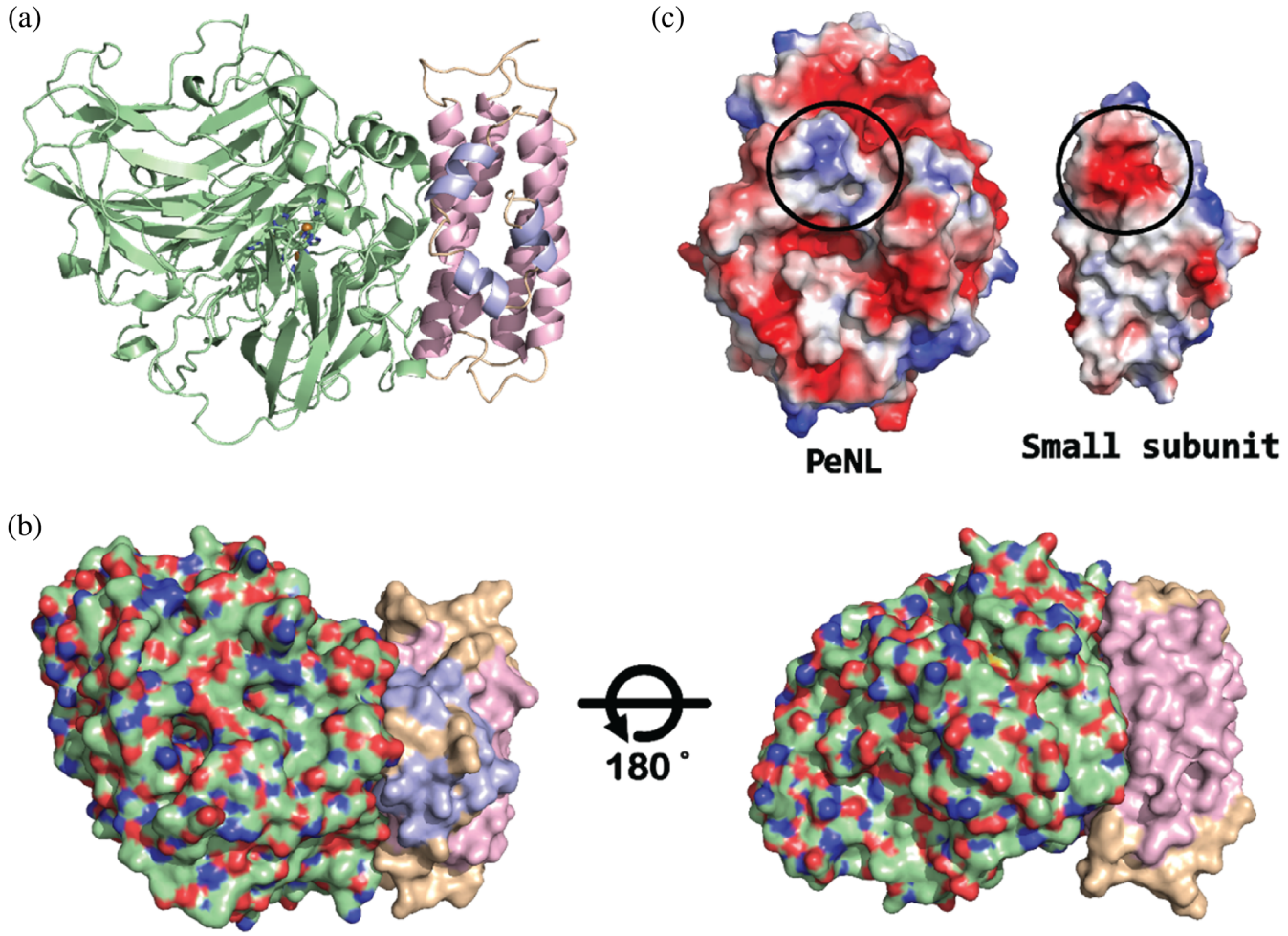

FIGURE 7 Structure prediction of PeNL-ss. (a) Structure prediction for PeNL-ss heterodimer. (b) Surface representation of the heterodimer. (c) Interaction surface of the large and the small subunits. The small subunit depicted in this figure is the crystal structure determined in this study.

PeNL-ss complex and 16,940 ± 340 Da for the small subunit. The results agree with the presence of a heterodimeric PeNL-ss complex in solution (molecular mass of the complex is ~72 kDa) and a monomeric small subunit in solution (molecular mass of ~17 kDa).

Structural and sequence alignments of the AlphaFold model of PeNL and the crystal structure of PM1L (PDB ID: 5ANH), a typical laccase sensu stricto crystallized and fully characterized by our group (De Salas et al., 2019; Pardo et al., 2016), are shown in Figure 8. A comparison of PeNL with several laccase PDBs showed that the first 90 hits present a RMSD (Root Mean Square Deviation) between 1.1 and 1.3 Å, indicating a high degree of similarity among all these structures. PM1L comes as the 15th hit of the DALI output (Holm et al., 2023). The alignment of 5ANH and the first hit (5Z22) shows no significant differences between them. Due to this high degree of similarity we decided to use 5ANH for the structural comparison, and we are confident that this comparison is valid as a canonical laccase sensu stricto.

The RMSD between PeNL and PM1L structures calculated using the program superpose from the CCP4 suite (Winn et al., 2011), for all atoms, is 0.951 Å, indicating that they are very similar. The structural alignment (Figure 8a) shows this high similarity except for five regions located on the protein surface (Zones 1–5), that showed significant differences between both structures. Some of these regions are next or include residues of the four substrate binding loops described in laccases, Loops 1–4 (Figure 8b). Zone 3 and 5 are located far from the active site and from the interaction surface with the small subunit. Zone 2 is located close to the entrance to the active site of the enzyme, in fact it contains most of Loop 2. Zone 4 is located on top of the T1 copper (Figure 8a). In PeNL Zone 4 is much shorter and includes most of Loop 4. Finally, Zone 1 presents 7 more residues in PeNL than in PM1L and is folded as an extra α-helix in the NLAC, whereas the shorter sequence in PM1L adopts a loop conformation (Figure 8a). The end of Zone 1 coincides with the beginning of Loop 1.

The interaction surface between the PeNL model and the small subunit crystal structure is shown in Figure 9. The interaction takes place between the bottom part of PeNL and mostly by the surface made up by helices α-1 and α-3 of the small subunit, together with some residues

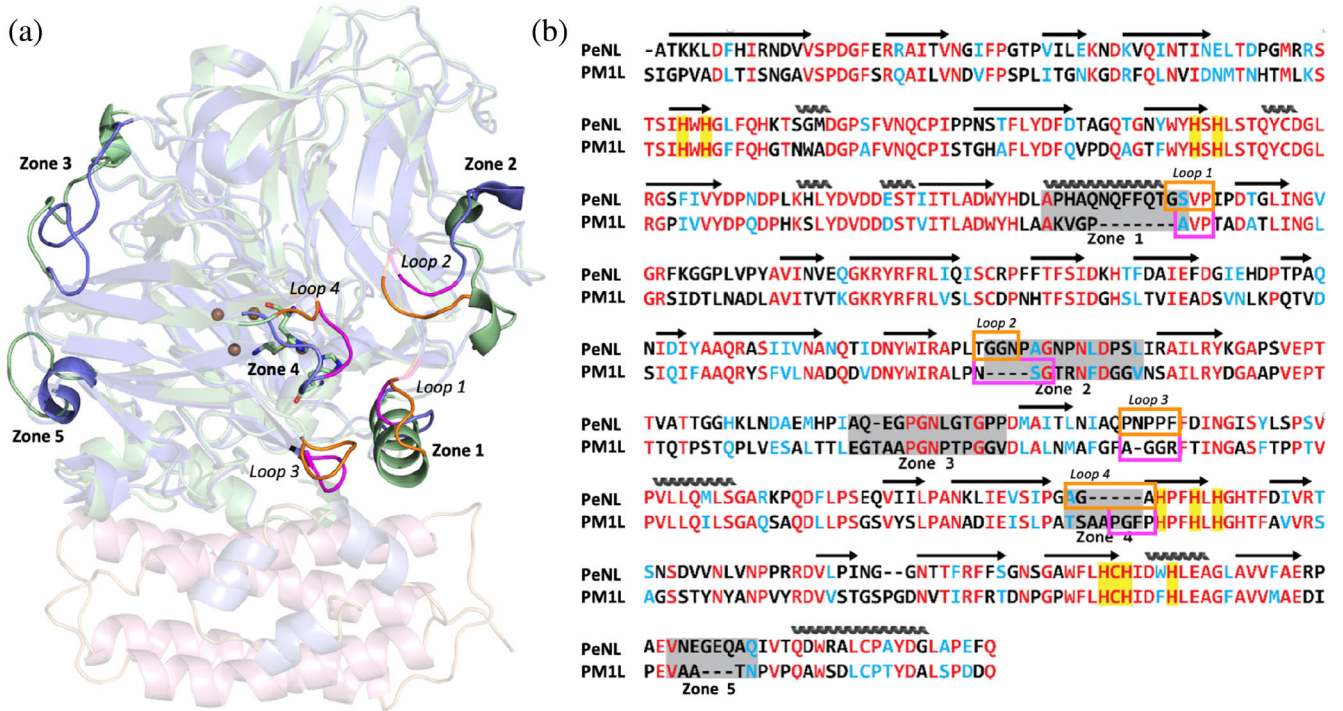

FIGURE 8 Comparison of the PeNL and PM1 laccase. (a) Structure alignment of PeNL model (palegreen) and PM1L crystal structure (slate). The five zones with significant structural differences are highlighted, as well as the four substrate binding loops (in orange for PeNL and magenta for PM1L). The small subunit is shown in lightpink, lightblue and wheat. The residues involved in T1 copper binding are shown as sticks and copper atoms as spheres. (b) Sequence alignment of PeNL and PM1L. Conserved residues are shown in red, residues with similar chemical characteristics in blue and non-conserved residues in black. The yellow boxes indicate the copper binding residues, the gray boxes indicate Zones 1–5, and the substrate-binding loops (Loops 1–4) are shown in orange (PeNL) or magenta (PM1L) boxes. Secondary structure of PeNL is shown on top of the sequence, arrows represent β-sheets and spirals represent α-helices.

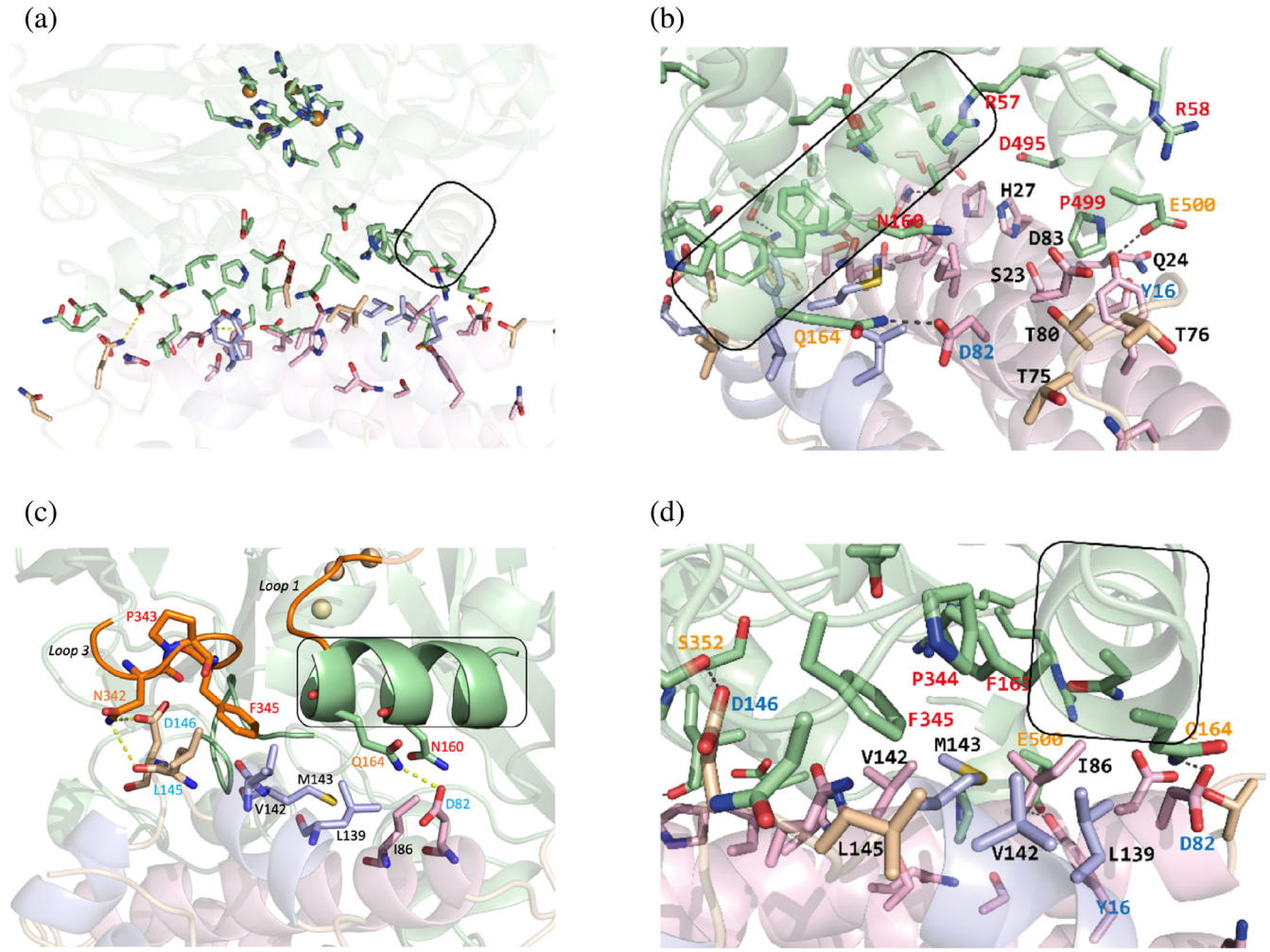

FIGURE 9 (a) Interaction surface between the PeNL model (palegreen) and the crystal structure of the small subunit (lightpink, lightblue and wheat). (b) Close view of the possible hydrogen bonds (dashed lines) formed between PeNL and the small subunit. (c) Close view of residues involved in polar and hydrophobic interactions of the extra α-helix (Zone 1, square, residues A155–T165) and Loop 3 of PeNL with the small subunit surface (d) Close view of a hydrophobic patch at the interaction surface. Residues from PeNL are numbered in red and from the small subunit in black. The interacting partners of the possible hydrogen bonds (dashed lines) are numbered in orange for PeNL and in blue for the small subunit.

from the loop connecting helices α-5 and α-6. This is the same surface that forms the homodimer in the crystal structure of the small subunit (Figure S5). The possible residues involved in the interaction are shown in Figure 9a. This extensive region is made up by hydrogen bond interactions (Figure 9b) and by hydrophobic patches (Figure 9d). There are four hydrogen bond interactions with distances below 3.1 Å (Figure 9, dashed lines), and one with a distance of 3.7 Å. The extra α-helix in PeNL (Zone 1, Figure 8) that is not present in the PM1L is involved in, at least, one hydrogen bond interaction between Q164 of PeNL and D82 of the small subunit (Figure 9b,c). Two other hydrogen bond interactions involve N342 from Loop 3 of PeNL with L145 and D146 of the small subunit. There are more possible interactions that could be mediated by water molecules or created by different conformations of the residues involved, but the model does not allow to predict this type of interactions. The real interactions will only be able to be known with a crystal structure of the heterodimer. This way we will know how the two interacting surfaces will change to accommodate each other.

3 | DISCUSSION

Fungal laccases are mostly monomeric enzymes (Hakulinen & Rouvinen, 2015; Zhukova et al., 2010), although some studies have described they can constitute functional heterodimers. The existence of these complexes was first described for the extensively studied POXA3 laccase of *P. ostreatus* (Palmieri et al., 2003). This

enzyme has been recently reclassified as a member of the NLAC family (Ruiz-Dueñas et al., 2021). The heterodimer of POXA3 consisted of a catalytic subunit (laccase-like enzyme) and a small subunit with no described enzymatic activity (Giardina et al., 2007). More recently, an equivalent heterodimeric complex was identified and characterized in *P. eryngii var. ferulae* (Zhang et al., 2021) whose laccase-like subunit has been reclassified as a NLAC in this study (see Figure S8). Despite there is no known catalytic activity associated to these small proteins, both studies agreed in the superior thermostability of the heterodimers compared to the monomeric enzymes (Faraco et al., 2008; Zhang et al., 2021). The fact that at least one gene of small subunit-like proteins is found in every studied genome encoding NLACs (Ruiz-Dueñas et al., 2021) suggests the formation of heterodimers is a general rule for this type of laccase-like enzymes.

The NLAC of *P. eryngii* retained over 50% of its initial activity after heat shock in the presence of the small subunit, whereas the enzyme alone was completely inactivated. The functional expression and stabilizing effect of the small protein was therefore evidenced, as well as its interaction with the NLAC, regardless of the small subunit was co-expressed with the enzyme or mixed during the co-growth of *A. oryzae* clones expressing both separately. The thermotolerance of PeNL-ss was higher in the presence of extra small subunit. This fact suggest that the small subunit was produced to a lesser extent than the large subunit by the *A. oryzae* clone co-transformed with both proteins, because the integrative homologous recombination does not ensure equal copy numbers for the two proteins.

The catalytic efficiency for ABTS oxidation ($k_{cat}/K_M = 980\ mM^{-1}\ s^{-1}$) of PeNL was relatively in the same range than those described for laccases sensu stricto from the fungi *Coprinopsis cinerea*, $k_{cat}/K_M = 214\ mM^{-1}\ s^{-1}$ (Wang et al., 2014); *Agrocybe pediades*, $k_{cat}/K_M = 7391\ mM^{-1}\ s^{-1}$ (Aza, Molpeceres, et al., 2021b); PM1, $k_{cat}/K_M = 26{,}106\ mM^{-1}\ s^{-1}$ (De Salas et al., 2019); *Trametes trogii*, $k_{cat}/K_M = 110\ mM^{-1}\ s^{-1}$ (Garzillo et al., 1998). Conversely, PeNL barely oxidized DMP and did not show activity on DMPD, two other laccase model substrates. This fact is most likely related to the presence in PeNL of R211, which is fully conserved among NLACs instead of the equivalent aspartic acid in laccases sensu stricto (Ruiz-Dueñas et al., 2021). The acidic residue has been demonstrated to assist the concerted electron-proton transfer during phenol oxidation (Galli et al., 2013). Its substitution had a critical impact in laccase catalytic efficiency for the oxidation of phenolic compounds (Madzak et al., 2006). The crucial role of this acidic residue in phenol oxidation was confirmed here by the remarkably higher activity of the PeNL $_{R211D}$ variant with DMP. This acidic residue also mediates by hydrogen-bond the interaction with aryl amines in the laccase binding pocket (Bertrand et al., 2002), thus explaining the poor oxidation of DMPD by PeNL.

The small subunit alone did not show laccase activity, but it enhanced the catalytic activity of PeNL with ABTS and DMP, in agreement with the enhancement of activity observed in other NLAC heterodimers (Faraco et al., 2008; Zhang et al., 2021). However, we provide for the first time kinetic constants for both the monomeric and heterodimeric forms of a NLAC. Despite the better catalytic activity of PeNL-ss heterodimer compared to PeNL alone, its activity toward phenols (and aryl-amines) was still remarkably low compared to laccases sensu stricto (Aza, Molpeceres, et al., 2021b; De Salas et al., 2019; Garzillo et al., 1998; Wang et al., 2014). Contradictory activity values are found in the literature regarding other NLAC heterodimers, although all of them coincide in the much better oxidation of ABTS than DMP, as shown here for PeNL. POXA3 exhibited high efficiency with DMP ($k_{cat}/K_M = 1666$ and $2333\ mM^{-1}\ s^{-1}$) and remarkably high activity with ABTS (Palmieri et al., 2003). By contrast, the laccase-like enzyme from *Pleurotus citrinopileatus* (PcLac2), reclassified as a NLAC (unpublished data), has worse catalytic efficiencies than PeNL with DMP ($k_{cat}/K_M = 0.051\ mM^{-1}\ s^{-1}$) or ABTS ($k_{cat}/K_M = 37\ mM^{-1}\ s^{-1}$) (Zerva et al., 2021).

The main effect attributed to the small subunit is to increase the thermal stability of NLAC through interaction in the heterodimeric complex (Faraco et al., 2008; Zhang et al., 2021). Our results confirm this effect by the remarkable increment in T50 (16°C) and the higher residual activities of PeNL-ss heterodimer over PeNL in the long-term incubation assay at different temperatures. The presence of the small protein also improved the stability of PeNL at acidic pH (Faraco et al., 2008; Zhang et al., 2021), as well as in the presence of organic solvents or protein denaturalizing agents such as SDS, two effects that had not been described previously. These results open new scenarios for the use of these small proteins to enhance the biotechnological potential as biocatalysts of laccase-like enzymes.

We have solved for the first time the helix-bundle crystal structure of a small subunit of a NLAC. Its functionality was demonstrated by the increment in thermal stability when it was added in vitro to PeNL. The small subunit forms a homodimer in the asymmetric unit of the crystal structure, but SEC-MALS analysis evidenced it is a monomer of 17 kDa in solution and forms a heterodimer of 77.4 kDa with PeNL. The most likely explanation for this discrepancy is the much higher protein

concentration in the crystal than in SEC-MALS assay, and that the presence of the hydrophobic surface formed by helices α-1 and α-3 drives the protein to form a dimer to enhance its stability by hiding the hydrophobic surfaces.

The model of PeNL-ss heterodimer showed a likely favorable interaction between the large and the small subunits through the same surface that forms the aforementioned homodimer in the crystal. Some of the putative interactions between both subunits involve residues from or in close proximity to the loops that determine the protein-substrate interactions in MCOs (Mehra et al., 2018; Pardo et al., 2016) One characteristic feature on PeNL is the presence of the α-helix in Zone 1, that is not present in the canonical laccase PM1L. This helix is involved in, at least, one hydrogen bond interaction with the small subunit. Zone 1 is adjacent to Loop 1 of the binding pocket, highlighting the possible influence of this secondary structure on the type of substrates that the enzyme can bind. Two others hydrogen bonds between the enzyme and the small subunit also involve residues of the substrate binding Loop 3. These findings could partially explain the catalytic differences experimentally observed between the monomeric PeNL or the heterodimer.

On the other hand, structural differences were found between PeNL and PM1L in regions far from the surface interaction between PeNL and the small subunit, but related to other substrate binding loops. Zone 4 in PeNL includes most of Loop 4, which is much shorter than in PM1L, indicating a very likely influence of this region on substrate binding. Zone 2 also includes the majority of Loop 2, with great variability between both MCOs. Particularly, the confidence for the prediction of the Zone 2 in PeNL is the lowest of the whole sequence (Figure S6). This together with the fact that it is also an external flexible loop (it contains three Gly, one Ala and one Ser out of 14 total residues) might indicate that this region could adopt different conformations. All these findings might explain the differences in activity between PeNL and laccases sensu stricto.

Although the role of NLACs in nature remains unclear, several secretomic studies indicated that they take part of the lignocelullosic enzymatic toolkit. Addition of alkali lignin in *P. eryngii* liquid cultures strongly induced the secretion of the laccase (Muñoz et al., 1997a) lately identified as a NLAC (Pleery1- ID 1521536) (Ruiz-Dueñas et al., 2021). Moreover, PeNL and the small subunit were upregulated in the transcriptome of *P. eryngii* grown on wheat straw. PeNL was also abundantly identified in the exoproteome of the fungus after several days of solid-state fermentation on wheat-straw, and the small subunit was also more expressed in the presence of the lignocellulosic material than in a minimal medium (Peña et al., 2021). Alike PeNL, when *P. ostreatus* was grown on woody lignocellulosic substrates, POXA3 was strongly induced together with other ligninolytic oxidoreductases, suggesting a key role in lignin degradation (Fernández-Fueyo et al., 2016). POXA3 transcript levels were also upregulated in submerged culture in the presence of lignin or lignin-derived aromatic compounds, although the small subunit was not regulated in a coordinated way with the catalytic subunit (Pezzella et al., 2013). On the other hand, the inefficient phenol and aryl amine oxidation observed here for monomeric or heterodimeric PeNL bring into question its role in lignin biodegradation. Interestingly, in a recent *Lentinula* study, and based on previous RNA-seq data from mycelium and fruiting bodies of *L. edodes* (Song et al., 2018), we observed that the MCO of this fungus classified here as a NLAC (Lentinedodes1-15,576 JGI, Figure S8) was up-regulated in the mycelium transcriptome but not in the fruiting body, which may indicate it participates in lignin modification during the vegetative growth (Sierra-Patev et al., 2022).

4 | CONCLUSIONS

NLACs are laccase-like enzymes that form heterodimers with small proteins of unknown function. In this study, the stability to different factors and the activity of the NLAC of *P. eryngii* were remarkably increased by the presence of the small subunit. The stabilizing effect of the latter was evident whether it was co-expressed with the enzyme or added exogenously, highlighting the PeNL-ss complex is formed in vivo and in vitro. We confirmed the complex is a heterodimer of 77.4 kDa, and predicted the interactions between the NLAC model and the crystal structure of the small subunit that has been solved here for the first time. PeNL exhibits distinctive structural features that are likely involved in substrate binding and/or the interaction with the small subunit, which could explain the differences in activity/stability of the monomeric or complexed PeNL, and in activity of the NLAC compared to a canonical laccase.

5 | MATERIALS AND METHODS

5.1 | Reagents and strain

The 2,6-Dimethoxyphenol (DMP), N,N-Dimethyl-1,4-phenylenediamine (DMPD) and Thrombin CleanCleave Kit were purchased from Sigma-Aldrich. High Pure Plasmid Isolation Kit and 2,2′-Azino-bis (3-ethylbenzothiazoline-6-sulfonic acid) (ABTS) were obtained from ROCHE. QIAquick gel extraction kit from Qiagen.

5.2 | Cloning and variants construction

The coding sequence (CDS) of PeNL used here differs from the native sequence (JGI ID 1521536) of *P. eryngii* ATCC 90797 in three consensus mutations (K220N, E478P, T484P) added to facilitate the heterologous expression of the enzyme (Aza, De Salas, et al., 2021a). The CDS of the small subunit (JGI ID: 1468497) was identified in JGI *P. eryngii* genome using the small subunit of POXA3 (GenBank ID: CAL64898) as a query sequence. The CDS of small subunit was synthesized the novo by Novozymes A/S, Denmark for expression in *A. oryzae*. Additionally, this CDS was optimized for *E. coli* expression by Optimized software (Puigbo et al., 2007), and cloned in the His-tag-containing pET28 plasmid between NdeI and BamHI cleavage sites by ATG:biosynthetics GmbH. $PeNL_{R211D}$ variant was obtained by In Vivo Overlap Extension (IVOE) in *S. cerevisiae* (Aza, Molpeceres, et al., 2021b) using external and internal primers described in Table S1.

5.3 | Heterologous protein production

Aspergillus oryzae: Both, PeNL and the small subunit were cloned by integrative homologous recombination separately (different *A. oryzae*) or together (same *A. oryzae*). Enzyme overexpression in *A. oryzae* (Matsui et al., 2016) was carried out at Novozymes A/S in standard MDU media supplemented with 2 mM $CuSO_4$. PeNL and PeNL-ss complex were purified as described (Aza et al., 2023). Laccases were analyzed by SDS–PAGE to confirm their purity. SDS–PAGE was performed in 12% polyacrylamide gels using dual color precision plus protein (Bio-Rad) as standard and Coomassie R-250 staining.

Escherichia coli: the small subunit was produced as soluble folded protein in flask cultures of BL21 (DE3) pLysS *E. coli* strain in lactose-containing autoinduction medium ZYM-5052 (Studier, 2005), grown for 4–5 days at 16°C. Cells were harvested (8–10 min at 5000*g*) and frozen for 24 h. Then, the pellet was resuspended in 50–70 mL of 50 mM Tris–HCl (pH 8) buffer, 0.3 M NaCl, and 20 mM imidazole. Cells were lysed with lysozyme (2 mg/mL), DNase, and sonication. After centrifugation (1 h 21,000*g*) soluble fractions were filtered with a 0.22 μm membrane.

The histidine-tagged small protein was purified by immobilized metal ion affinity chromatography with HiTrap IMAC FF 5-mL column (Cytiva), preloaded with 0.1 M $NiSO_4$, using an Äkta (GE Healthcare) fast protein liquid chromatography (FPLC) system. Sample was injected with 50 mM Tris–HCL (pH 8) buffer, 0.3 M NaCl, and 20 mM imidazole and eluted with 1 M imidazole buffer using a linear gradient (0–50%). Then, the His-tag was removed from the protein using the Thrombin CleanCleave Kit following the manufacturer indications, and the protein was finally purified through a second affinity chromatography run with HiTrap IMAC FF 5-mL column by collecting the non-retained protein.

Saccharomyces cerevisiae: Yeast cells transformed with a plasmid containing PeNL or $PeNL_{R211D}$ genes and grown at 20°C as described (Aza, Molpeceres, et al., 2021b). When maximum activity was reached, cells were centrifuged (5000 rpm, 4°C) and supernatants concentrated with Amicon Ultra Centrifugal filters (30 kDa MWCO) at 5000 rpm, 10 min.

5.4 | Activity determination in flask cultures

After 72 hours of *A. oryzae* flask cultures and co-cultures, samples were harvested and the laccase activity in the extracellular fraction determined using 3 mM ABTS ($\varepsilon_{418} = 36{,}000\ M^{-1}\ cm^{-1}$) in 100 mM Citrate–Phosphate (CP) buffer at pH 4, in 96-well plates using a SpectraMax M2 plate reader. For thermotolerance assays, aliquots were incubated for 10 min at 50°C and the residual activity measured with 3 mM ABTS in 100 mM buffer CP.

5.5 | Biochemical characterization

All assays were carried out in 96-well plates using a SpectraMax M2 plate reader.

T50 assay was performed as described (Aza, Molpeceres, et al., 2021b) in buffer CP. T50 is defined as the temperature at which the enzyme retains 50% of the initial activity after 10 min.

Thermal stability. Enzyme samples were diluted in 20 mM Tris–HCl buffer at pH 7.0 to a final concentration of 1 U/L ABTS. After 0.5, 1, 3, 5, and 24 h of incubation at 30, 40, and 50°C, 20 μL-aliquots were added to 96-well plates (triplicates) and tempered to RT before 180 μL of 3 mM ABTS in buffer CP were added, and residual activity was measured.

Long-term stability to pH and co-solvent were measured as described (Aza, Molpeceres, et al., 2021b) at 20°C, and ABTS activity was measured in buffer CP. Enzyme stability was assayed in triplicate as described for pH stability, but using purified enzyme incubated in 20 mM Tris–HCl buffer at pH 7.4 at 10°C with 40% and 60% ethanol and DMSO or 0.1% SDS (v/v). The activity of the enzyme at time zero in the presence of the co-solvent was taken as 100% activity for evaluating the enzyme stability within time.

Optimal pH activity was measured using 20 μL of the concentrated supernatants (at 1 U/mL) and 180 μL of 3 mM ABTS in 100 mM Britton Robinson (BR) buffer at pH 3–8 range. The solution was mixed and measured in kinetic mode in triplicate. Relative activities were calculated respecting the maximum activity of each laccase variant.

Catalytic constants were determined using 0.005–4 mM of ABTS, 0.05–60 mM of DMP and 0.05–5 mM of DMPD in 100 mM buffer CP at pH 5 for ABTS and DMPD and at pH 5 for DMPD. To calculate K_M and k_{cat} values the average V_{max} was represented *versus* substrate concentration and fitted to a single rectangular hyperbola function in SigmaPlot (version 14.0) software for DMP and DMPD, and fitted to a Hill-sigmoidal for ABTS, where parameter a represents k_{cat} and parameter b represents K_M. In all assays three replicates of each laccase variant were used.

In vitro formation of PeNL-ss heterodimer. Purified PeNL produced in *A. oryzae* was incubated with the pure small subunit produced in *E. coli* in 20 mM Tris–HCl buffer at pH 7 during 5 min at RT. As negative control, another aliquot of PeNL was incubated alone in the same conditions. Then, both samples were incubated at 60°C for 5 min, tempered for 10 min at RT, and the residual activities measured with 3 mM ABTS in buffer CP.

PeNL and PeNL$_{R211D}$. The DMP oxidation activities of concentrated supernatants from *S. cerevisiae* cultures were measured (triplicate reactions) by adding 20 μL of 1 U/mL laccase supernatant (with ABTS at pH 3) to 180 μL of 10 mM DMP in acetate phosphate pH 5.

5.6 | Protein quantification

Protein was quantified using a Qubit 3.0 fluorometer from Sigma-Aldrich.

5.7 | Crystallization and data collection of the small subunit

Crystallization trials were performed at 295 K using the sitting-drop vapor-diffusion method with commercial screening solutions in 96-well sitting-drop plates (Swissci MRC; Jena Bioscience, Jena, Germany). Drops were set up by mixing equal volumes (0.2 μL) of a protein solution (9.5 mg/mL) and reservoir solution using an Oryx 4 (Douglas Instruments Ltd., East Garston, UK) nano-dispenser robot and equilibrated against 50 μL reservoir solution. Crystals of the protein appeared overnight in 0.1 M Imidazole at pH 8.0, 2.5 M NaCl. For data collection, crystals were harvested in 0.1 M Imidazole at pH 8.0, 2.5 M NaCl and 35% ethylene glycol and flash-cooled in liquid nitrogen. X-Ray data collection was performed at the ALBA Synchrotron (Cerdanyola del Vallès, Spain) BL13 XALOC beamLine. Data were indexed and integrated, scaled and merged using XDS mL (Kabsch & Max-Planck-Institut, 1993).

5.8 | Structure determination of the small subunit

Protein structure was solved by molecular replacement using the AlphaFold2 model (Jumper et al., 2021; Varadi et al., 2022) with Phaser (McCoy et al., 2007). The initial model was first refined using Phenix (Liebschner et al., 2019) and alternating manual building with Coot (Emsley et al., 2010). The final model was obtained by repetitive cycles of refinement; solvent molecules were added automatically and inspected visually for chemically plausible positions. The stereochemical quality of the model was assessed with MolProbity (Chen et al., 2010). The structural figures were generated using the PyMOL program (http://www.pymol.org). Data processing and refinement statistics are listed in Table S2.

5.9 | Predicted structure of the PeNL-ss complex

The prediction of the quaternary structure of the complex formed by the small and the catalytic subunits was carried out using AlphaFold2 (Jumper et al., 2021; Varadi et al., 2022). Additionally, we used the PDB of the crystal structure of the small subunit for representation of the complex in the corresponding figures. Comparison of PeNL model with PM1L structure (5ANH. PDB) was performed using the program superpose from the CCP4 suite (Winn et al., 2011).

5.10 | Size exclusion chromatography-multi angle light scattering

The experiments were performed using a Superdex 200 10/300 GL column (Cytiva) attached in-line to a DAWN-HELEOS light scattering detector and, in parallel, to an Optilab rEX refractive index detector (Wyatt Technology). Protein samples (200 μL) with concentrations ranging from 0.3 to 5 mg/mL were injected into the size exclusion column equilibrated with 20 mM Tris–HCL pH 7.5, 100 mM NaCL, and the chromatography process was carried out at RT with a flow rate of 0.5 mL/min. Data acquisition and analysis were performed using

ASTRA software (Wyatt) to calculate the molecular weight (MW) of the protein species that eluted from the column.

5.11 | Multiple sequence alignment and phylogenetic tree

The Multiple sequence alignment and phylogenetic tree of seven NLACs and ten laccase sensu stricto sequences from different orders of basidiomycete fungi that are available at the DOE JGI MycoCosm portal was performed as described (Aza et al., 2023). The ID of the predicted amino acid sequences and their fungal sources are depicted in the caption of Figure S7.

AUTHOR CONTRIBUTIONS

Pablo Aza: Investigation, methodology, data curation, writing—original draft. **Dolores Linde**: *E. coli* expression (supervision, methodology). **Gonzalo Molpeceres**: Phylogeny (data curation, software, validation). **Jesper Vind**: *A. oryzae* expression (supervision, methodology). **F. Javier Medrano**: Crystallization and protein structure (investigation, methodology and writing—review & editing). **Susana Camarero**: Conceptualization of the work, supervision, writing—review & editing, funding acquisition. All authors have read and agreed to the published version of the manuscript.

ACKNOWLEDGMENTS

This work was supported by the WoodZymes project funded by the Bio-based Industries Joint Undertaking (BBI JU) under GA 792070. The BBI JU received support from the EU's H2020 research and innovation programme and the Bio Based Industries Consortium. The work was also supported by GENOBIOREF project funded by MINECO/FEDER (BIO2017-86559-R), the LIG2PLAST project funded by MCIN/AEI/FEDER (PID2021-126384OB-I00), and the CSIC Interdisciplinary Platform for Sustainable Plastics toward a Circular Economy (PTI-SusPlast+). Pablo Aza acknowledges an FPU Grant from the Spanish Ministry of Universities including the grant for his short term stay at Novozymes. G. Molpeceres thanks the Tatiana Pérez de Guzmán el Bueno Foundation for his Predoctoral Environment Grant. We cordially thank the staff of beamline BL13-XALOC (Alba Synchrotron) for their generous and much appreciated support and the CIB Molecular Interaction Service for SEC-MALS analysis.

CONFLICT OF INTEREST STATEMENT

The authors declare no conflict of interest.

ORCID

Susana Camarero https://orcid.org/0000-0002-2812-895X

REFERENCES

Aza P, De Salas F, Molpeceres G, Rodríguez-Escribano D, De La Fuente I, Camarero S. Protein engineering approaches to enhance fungal laccase production in *S. cerevisiae*. Int J Mol Sci. 2021a;22(3):1–19. https://doi.org/10.3390/ijms22031157

Aza P, Molpeceres G, Ruiz-Dueñas FJ, Camarero S. Heterologous expression, engineering and characterization of a novel laccase of agrocybe pediades with promising properties as biocatalyst. J Fungi. 2021b;7(5):359. https://doi.org/10.3390/jof7050359

Aza P, Molpeceres G, Vind J, Camarero S. Multicopper oxidases with laccase-ferroxidase activity: classification and study of ferroxidase activity determinants in a member from Heterobasidion annosum s. l. Comput Struct Biotechnol J. 2023;21:1041–53. https://doi.org/10.1016/j.csbj.2023.01.030

Baldrian P. Fungal laccases-occurrence and properties. FEMS Microbiol Rev. 2006;30(2):215–42. https://doi.org/10.1111/j.1574-4976.2005.00010.x

Bertrand T, Jolivalt C, Briozzo P, Caminade E, Joly N, Madzak C, et al. Crystal structure of a four-copper laccase complexed with an arylamine: insights into substrate recognition and correlation with kinetics. Biochemistry. 2002;41(23):7325–33. https://doi.org/10.1021/bi0201318

Cambria MT, Gullotto D, Garavaglia S, Cambria A. In silico study of structural determinants modulating the redox potential of Rigidoporus lignosus and other fungal laccases. J Biomol Struct Dynamics. 2012;30(1):89–101. https://doi.org/10.1080/07391102.2012.674275

Chen VB, Arendall WB, Headd JJ, Keedy DA, Immormino RM, Kapral GJ, et al. MolProbity: all-atom structure validation for macromolecular crystallography. Acta Crystallogr D Biol Crystallogr. 2010;66(1):12–21. https://doi.org/10.1107/S0907444909042073

De Salas F, Camarero S. Fungal laccases as biocatalysts for wide range applications. In: Zaragoza O, Casadevall A, editors. Encyclopedia of mycology. The Netherlands: Elsevier; 2021. p. 233–46.

De Salas F, Cañadas R, Santiago G, Virseda-Jerez A, Vind J, Gentili P, et al. Structural and biochemical insights into an engineered high-redox potential laccase overproduced in aspergillus. Int J Biol Macromol. 2019;141:855–66. https://doi.org/10.1016/j.ijbiomac.2019.09.052

De Salas F, Pardo I, Salavagione HJ, Aza P, Amougi E, Vind J, et al. Advanced synthesis of conductive polyaniline using laccase as biocatalyst. PloS One. 2016;11(10):1–18. https://doi.org/10.1371/journal.pone.0164958

Emsley P, Lohkamp B, Scott WG, Cowtan K. Features and development of coot. Acta Crystallogr D Biol Crystallogr. 2010;66(4):486–501. https://doi.org/10.1107/S0907444910007493

Faraco V, Ercole C, Festa G, Giardina P, Piscitelli A, Sannia G. Heterologous expression of heterodimeric laccase from Pleurotus ostreatus in Kluyveromyces lactis. Appl Microbiol Biotechnol. 2008;77(6):1329–35. https://doi.org/10.1007/s00253-007-1265-5

Fernández-Fueyo E, Ruiz-Dueñas FJ, López-Lucendo MF, Pérez-Boada M, Rencoret J, Gutiérrez A, et al. A secretomic view of

woody and nonwoody lignocellulose degradation by Pleurotus ostreatus. Biotechnol Biofuels. 2016;9(1):1–18. https://doi.org/10.1186/s13068-016-0462-9

Ferraroni M, Scozzafava A, Ullah S, Tron T, Piscitelli A, Sannia G. Crystallization and preliminary X-ray crystallographic analysis of the small subunit of the heterodimeric laccase POXA3b from Pleurotus ostreatus. Acta Crystallogr F Struct Biol Commun. 2014;70(1):76–9. https://doi.org/10.1107/S2053230X13032810

Galli C, Madzak C, Vadalà R, Jolivalt C, Gentili P. Concerted electron/proton transfer mechanism in the oxidation of phenols by laccase. Chembiochem. 2013;14(18):2500–5. https://doi.org/10.1002/cbic.201300531

Garzillo AMV, Colao MC, Caruso C, Caporale C, Celletti D, Buonocore V. Laccase from the white-rot fungus Trametes trogii. Appl Microbiol Biotechnol. 1998;49(5):545–51. https://doi.org/10.1007/s002530051211

Giardina P, Autore F, Faraco V, Festa G, Palmieri G, Piscitelli A, et al. Structural characterization of heterodimeric laccases from Pleurotus ostreatus. Appl Microbiol Biotechnol. 2007;75(6):1293–300. https://doi.org/10.1007/s00253-007-0954-4

Giardina P, Faraco V, Pezzella C, Piscitelli A, Vanhulle S, Sannia G. Laccases: a never-ending story. Cell Mol Life Sci. 2010;67(3):369–85. https://doi.org/10.1007/s00018-009-0169-1

Hakulinen N, Rouvinen J. Three-dimensional structures of laccases. Cell Mol Life Sci. 2015;72(5):857–68. https://doi.org/10.1007/s00018-014-1827-5

Holm L, Laiho A, Toronen P, Salgado M. DALI shines a light on remote homologs: one hundred discoveries. Protein Sci. 2023;23:e4519.

Janusz G, Pawlik A, Świderska-Burek U, Polak J, Sulej J, Jarosz-Wilkołazka A, et al. Laccase properties, physiological functions, and evolution. Int J Mol Sci. 2020;21(3):966. https://doi.org/10.3390/ijms21030966

Jones SM, Solomon EI. Electron transfer and reaction mechanism of laccases. Cell Mol Life Sci. 2015;72(5):869–83. https://doi.org/10.1007/s00018-014-1826-6.Electron

Jumper J, Evans R, Pritzel A, Green T, Figurnov M, Ronneberger O, et al. Highly accurate protein structure prediction with AlphaFold. Nature. 2021;596(7873):583–9. https://doi.org/10.1038/s41586-021-03819-2

Kabsch W. Integration, scaling, space-group assignment and post-refinement. Acta Cryst. Section D-Biological crystallography. 2010;66:133–44. https://doi.org/10.1107/S0907444909047374

Krissinel E, Henrick K. Inference of macromolecular assemblies from crystalline state. J Mol Biol. 2007;372(3):774–97. https://doi.org/10.1016/j.jmb.2007.05.022

Kumar SVS, Phale PS, Durani S, Wangikar PP. Combined sequence and structure analysis of the fungal laccase family. Biotechnol Bioeng. 2003;83(4):386–94. https://doi.org/10.1002/bit.10681

Liebschner D, Afonine PV, Baker ML, Bunkoczi G, Chen VB, Croll TI, et al. Macromolecular structure determination using X-rays, neutrons and electrons: recent developments in phenix. Acta Crystallogr D Struct Biol. 2019;75:861–77. https://doi.org/10.1107/S2059798319011471

Madzak C, Mimmi MC, Caminade E, Brault A, Baumberger S, Briozzo P, et al. Shifting the optimal pH of activity for a laccase from the fungus Trametes versicolor by structure-based mutagenesis. Protein Eng Des Sel. 2006;19(2):77–84. https://doi.org/10.1093/protein/gzj004

Matsui T, Udagawa H, Kishishita S, Skovlund D. Patent No. WO2016026938A1. 2016.

McCoy AJ, Grosse-Kunstleve RW, Adams PD, Winn MD, Storoni LC, Read RJ. Phaser crystallographic software. J Appl Cryst. 2007;40(4):658–74. https://doi.org/10.1107/S0021889807021206

Mehra R, Muschiol J, Meyer AS, Kepp KP. A structural-chemical explanation of fungal laccase activity. Sci Rep. 2018;8(1):1–16. https://doi.org/10.1038/s41598-018-35633-8

Muñoz C, Guillén F, Martínez AT, Martínez MJ. Induction and characterization of laccase in the ligninolytic fungus *Pleurotus eryngii*. Curr Microbiol. 1997a;34(1):1–5. https://doi.org/10.1007/s002849900134

Muñoz C, Guillén F, Martínez AT, Martínez MJ. Laccase isoenzymes of *Pleurotus eryngii*: characterization, catalytic properties, and participation in activation of molecular oxygen and Mn2+ oxidation. Appl Environ Microbiol. 1997b;63(6):2166–74. https://doi.org/10.1128/aem.63.6.2166-2174.1997

Palmieri G, Cennamo G, Faraco V, Amoresano A, Sannia G, Giardina P. Atypical laccase isoenzymes from copper supplemented *Pleurotus ostreatus* cultures. Enzyme Microb Technol. 2003;33(2–3):220–30. https://doi.org/10.1016/S0141-0229(03)00117-0

Pardo I, Santiago G, Gentili P, Lucas F, Monza E, Medrano FJ, et al. Re-designing the substrate binding pocket of laccase for enhanced oxidation of sinapic acid. Catal Sci Technol. 2016;6(11):3900–10. https://doi.org/10.1039/c5cy01725d

Peña A, Babiker R, Chaduli D, Lipzen A, Wang M, Chovatia M, et al. A multiomic approach to understand how pleurotus eryngii transforms non-woody lignocellulosic material. J Fungi. 2021;7(6):426. https://doi.org/10.3390/jof7060426

Pezzella C, Lettera V, Piscitelli A, Giardina P, Sannia G. Transcriptional analysis of *Pleurotus ostreatus* laccase genes. Appl Microbiol Biotechnol. 2013;97(2):705–17. https://doi.org/10.1007/s00253-012-3980-9

Piscitelli A, Pezzella C, Giardina P, Faraco V, Sannia G. Heterologous laccase production and its role in industrial applications Alessandra. Bioeng Bugs. 2010;1(4):252–62.

Puigbo P, Guzman E, Romeu A, Garcia-Vallve S. OPTIMIZER: a web server for optimizing the codon usage of DNA sequences. Nucleic Acids Res. 2007;35:W126–31. https://doi.org/10.1093/nar/gkm219

Riva S. Laccases: blue enzymes for green chemistry. Trends Biotechnol. 2006;24(5):219–26. https://doi.org/10.1016/j.tibtech.2006.03.006

Ruiz-Dueñas FJ, Barrasa JM, Sánchez-García M, Camarero S, Miyauchi S, Serrano A, et al. Genomic analysis enlightens Agaricales lifestyle evolution and increasing peroxidase diversity. Mol Biol Evol. 2021;38(4):1428–46. https://doi.org/10.1093/molbev/msaa301

Sekretaryova A, Jones SM, Solomon EI. O2 reduction to water by high potential multicopper oxidases: contributions of the T1 copper site potential and the local environment of the trinuclear copper cluster. J Am Chem Soc. 2019;141(28):11304–14. https://doi.org/10.1021/jacs.9b05230

Shleev SV, Morozova OV, Nikitina OV, Gorshina ES, Rusinova TV, Serezhenkov VA, et al. Comparison of physico-chemical characteristics of four laccases from different basidiomycetes.

Biochimie. 2004;86(9–10):693–703. https://doi.org/10.1016/j.biochi.2004.08.005

Sierra-Patev S, Byoungnam M, Naranjo-Ortiz M, Looney B, Konkelc Z, Hibbett D. A global phylogenomic analysis of the shiitake genus Lentinula. Proc Natl Acad Sci. 2022;120(10):e2214076120. https://doi.org10.1073/pnas.2214076120

Song HY, Kim DH, Kim JM. Comparative transcriptome analysis of dikaryotic mycelia and mature fruiting bodies in the edible mushroom Lentinula edodes. Sci Rep. 2018;8(1):1–15. https://doi.org/10.1038/s41598-018-27318-z

Studier FW. Protein production by auto-induction in high density shaking cultures. Protein Expr Purif. 2005;41(1):207–34. https://doi.org/10.1016/j.pep.2005.01.016

Varadi M, Anyango S, Deshpande M, Nair S, Natassia C, Yordanova G, et al. AlphaFold protein structure database: massively expanding the structural coverage of protein-sequence space with high-accuracy models. Nucleic Acids Res. 2022;50(D1):D439–44. https://doi.org/10.1093/nar/gkab1061

Wang B, Wang L, Lin Y, Han Q, Han J, Gao J, et al. Purification and characterization of a laccase from Coprinopsis cinerea in Pichia pastoris. World J Microbiol Biotechnol. 2014;30(4):1199–206. https://doi.org/10.1007/s11274-013-1540-9

Winn MD, Ballard CC, Cowtan KD, Dodson EJ, Emsley P, Evans PR, et al. Overview of the CCP4 suite and current developments. Acta Crystallogr. 2011;D67:235–42.

Xu F. Oxidation of phenols, anilines, and benzenethiols by fungal laccases: correlation between activity and redox potentials as well as halide inhibition. Biochemistry. 1996;35(23):7608–14. https://doi.org/10.1021/bi952971a

Xu F, Berka RM, Wahleithner JA, Nelson BA, Shuster JR, Brown SH, et al. Site-directed mutations in fungal laccase: effect on redox potential, activity and pH profile. Biochem J. 1998;334(1):63–70. https://doi.org/10.1042/bj3340063

Zerva A, Pentari C, Termentzi A, America AHP, Zouraris D, Bhattacharya SK, et al. Discovery of two novel laccase-like multicopper oxidases from Pleurotus citrinopileatus and their application in phenolic oligomer synthesis. Biotechnol Biofuels. 2021;14(1):1–16. https://doi.org/10.1186/s13068-021-01937-7

Zhang Q, Yuan C, Wang F, Xu S, Li Y, Shi G, et al. Roles of small subunits of laccase (ssPOXA3a/b) in laccase production by Pleurotus eryngii var. ferulae. J Agric Food Chem. 2021;69(44):13113–24. https://doi.org/10.1021/acs.jafc.1c04777

Zhukova YN, Lyashenko AV, Lashkov AA, Gur'Yanov VA, Kobyl'skaya YV, Zhukhlistova NE, et al. Atomic structure of unligated laccase from Cerrena maxima at 1.76 Å with molecular oxygen and hydrogen peroxide. Crystallogr Rep. 2010;55(3):436–47. https://doi.org/10.1134/S1063774510030120

SUPPORTING INFORMATION

Additional supporting information can be found online in the Supporting Information section at the end of this article.

How to cite this article: Aza P, Linde D, Molpeceres G, Vind J, Medrano FJ, Camarero S. Role and structure of the small subunit forming heterodimers with laccase-like enzymes. Protein Science. 2023;32(9):e4734. https://doi.org/10.1002/pro.4734